

Unraveling the Influence of Li⁺-cation and TFSI⁻-anion in Poly(ionic liquid) Binders for Lithium-Metal Batteries

Rafael Del Olmo,^[a] Gregorio Guzmán-González,^{*[b]} Ilda O. Santos-Mendoza,^[c] David Mecerreyes,^[a, d] Maria Forsyth,^[a, d, e] and Nerea Casado^{*[a, d]}

Ion transport in composite electrodes plays a key role in the electrochemical performance of lithium-metal batteries (LMBs), particularly at high current densities, and hence, some works have suggested the use of ionic conducting polymers as binders. Herein, in order to assess the importance of the type of ion conduction in binders, two poly(ionic liquid) polymers were analyzed as binders in LiFePO₄ (LFP) cathodes: poly(lithium 1-[3-(methacryloyloxy)propylsulfonyl]-1-(trifluoromethane sulfonyl) imide) (PMTFSI-Li), and poly(diallyldimethylammonium bis(trifluoromethane sulfonyl)imide) (PDADMA-TFSI). Their functionalities allow modulating the individual transport of their counter-ions, Li⁺ and TFSI⁻, respectively; in comparison with conventional PVDF binder. Thus, LFP-C-Binder cathodes,

namely C-PVDF, C-PDADMA-TFSI and C-PMTFSI-Li, were evaluated in LMBs. C-PMTFSI-Li exhibited the best performance reaching the theoretical specific capacity ($170.3 \pm 0.8 \text{ mAh g}^{-1}$) at C/10, an outstanding capacity at 10 C ($100.6 \pm 0.5 \text{ mAh g}^{-1}$), and long lifespan (> 500 cycles at 1 C). C-PDADMA-TFSI showed good long-term cycling and high performance at high C-rate, while C-PVDF ended up fading before reaching 500 cycles. Surprisingly, it was observed that the presence of ionic binders into the cathode formulation influenced on Li⁰ metal deposition morphology, leading to a more homogeneous plating (specially PMTFSI-Li) in comparison with PVDF; and therefore, exhibiting a mitigation of mossy lithium growth.

Introduction

Due to the exponential increase of world's energy demand during the last decades and the transition to a climate-neutral society, research on energy storage has focused on improving the performance of actual devices to increase the efficiency and range of power electronics and electric vehicles.^[1,2] Among the electrochemical energy storage technologies, batteries, supercapacitors, and pseudo-capacitors stand out, in particular lithium-ion batteries (LIB), which offer high energy density and light-weight devices.^[3,4] So far, most of the portable electronics, electric vehicles, and renewable energy storage grids are supported by this technology, which is continuously growing, and thereby, the enhancement of energy density, rate capability, and cycle life has become a priority for these energy storage devices.

Currently, lithium-metal batteries (LMB) are getting attention because of their high theoretical capacity.^[5] Cathodes in LMBs are composed of a redox-active material, responsible for the charge storage in the electrodes (LiFePO₄, LiNi_xMn_yCo_zO₂, LiCoO₂ among others), electronic conducting agents (i.e., carbon or electronic conducting polymers), and a polymer that acts as binder [commonly poly(vinylidene fluoride), PVDF].^[6] Today, one of the main challenges facing this type of battery is to obtain the maximum real specific capacity and capacity retention during long-term cycling tests where parameters such as active material particle size, electronic conductivity, porosity, electrolyte, and ionic conductivity play an important role in the electrochemical performance of composite electrodes. As an example, Winter and co-workers inspected the impact of carbon particle size on the battery performance of LiFePO₄/C nanocomposites.^[7] The results showed that the overall conductivity increased with increasing carbon surface area because smaller carbon particles can create more contact points with LiFePO₄ improving the electronic transport.

Besides, the porosity of the final electrode must be optimized to facilitate Li⁺ transport, as the Li⁺ transport from the electrolyte to the active material takes place due to the absorption of liquid electrolyte into the electrode surface. Moreover, it has been demonstrated that the interaction of the carbon coating and the binder has a considerable impact on the mechanism of charge transfer, which could be a determining factor in the performance of lithium batteries, mainly at high charge/discharge rates.^[8,9] In this regard, the choice of the binder can be crucial to determine the performance of composite electrodes and in general of lithium based batteries.^[8,10] Trends in the development of polymeric materials

[a] Dr. R. Del Olmo, Prof. D. Mecerreyes, Prof. M. Forsyth, Dr. N. Casado POLYMAT, University of the Basque Country UPV/EHU. Joxe Mari Korta Center, Tolosa 72, 20018 Donostia-San Sebastián, Spain
E-mail: nerea.casado@ehu.eus

[b] Prof. G. Guzmán-González Departamento de Química, Universidad Autónoma Metropolitana-Iztapalapa, 09340, México City, México
E-mail: gregguzmn@gmail.com

[c] Dr. I. O. Santos-Mendoza Laboratoire de Réactivité et de Chimie des Solides, Université de Picardie Jules Verne, CNRS UMR7314, 15 Rue Baudelocque, 80039 Amiens, France

[d] Prof. D. Mecerreyes, Prof. M. Forsyth, Dr. N. Casado Ikerbasque, Basque Foundation for Science, 48011, Bilbao, Spain

[e] Prof. M. Forsyth Institute for Frontier Materials (IFM), Deakin University, Burwood, Victoria 3125, Australia

 Supporting information for this article is available on the WWW under <https://doi.org/10.1002/batt.202200519>

as binder include water-processable polymers and biopolymers,^[1,11,12] as well as the use of ionic polymers, such as single-ion conducting polymers (SICP) and poly(ionic liquid)s (PIL)s. As an example, Xu et al. found that the use of carboxymethyl cellulose (CMC) polyelectrolyte as binder for NMC/C-based cathodes diminished the overpotential in comparison with PVDF, which was critical for long-term cyclability.^[13] In addition to that, some works have reported the benefits of using functionalized binders which have electronic conductive properties, providing a more intimate electronic contact between redox-active compounds and the current collector.^[14,15] On the other hand, the use of single-ion conduction polymers as binders (binderlyte) has been suggested to overcome ion transport limitations in the cathode and therefore, improve cell performances.^[16–18] It has been recently published new binderlytes for Li|NMC(111) cells with superior cycling stability and capacity retention than conventional formulations for liquid- and solid-state devices.^[19,20] Some poly(ionic liquids) based on mobile TFSI⁻ have also been employed as binders, looking for facilitating Li⁺ conduction pathways, observing a more stable cycling and higher specific capacities in LFP/C cathodes.^[21] However, the role of the type of mobile ion (cationic or anionic) in polymeric binders and their behavior in contact with conventional liquid electrolytes has not been investigated in detail so far.

In this work, LiFePO₄/C based cathodes were prepared using two different poly(ionic liquid) polymers: poly(diallyldimethylammonium bis(trifluoromethanesulfonyl)imide (PDADMA-TFSI) and poly(lithium 1-[3-(methacryloyloxy) propylsulfonyl]-1-(trifluoromethanesulfonyl) (PMTFSI-Li) as binders (see Figure 1) and labeled as C-PMTFSI-Li and C-PDADMA-TFSI, respectively. These polymers were chosen as ionic conducting binders for LFP/C cathodes to provide suitable conditions to elucidate the role of TFSI⁻ and Li⁺ ions transport within the composite electrode on the overall electrochemical performance of the cells. Moreover,

the selected ionic polymers present an excellent solubility in acetone (PDADMA-TFSI) and water (PMTFSI-Li) facilitating their recyclability for a second life application of this binder material.^[22] The electrodes were cycled using 1 M LiTFSI in DOL:DME (1:1 v/v) as electrolyte and compared with conventional LFP/C/PVDF electrodes in terms of cyclic voltammetry, cyclability, cycle life, and electrochemical impedance spectroscopy (EIS).

Results and Discussion

Electrolyte uptake

PDADMA-TFSI and PMTFSI-Li were used as binders in LiFePO₄/C based cathodes to assess the importance of ion transport (TFSI⁻ in PDADMA-TFSI and Li⁺ in PMTFSI-Li) within the cathode structure. The electrochemical performances were compared to a cell containing the commonly used non-conductive PVDF binder. In traditional lithium-ion batteries with non-conductive binders, liquid electrolyte penetrates into the pores of the cathode providing ionic conduction through the electrode. In order to evaluate the wettability of cathodes with the different binders, electrolyte absorption was evaluated (Figure 2). For this purpose, pristine electrodes (LFP/C65/binder 80/10/10 wt.%) were soaked separately in fresh electrolyte (0.5 mL) for short (5 seconds) and long (48 h) immersion times in closed vials independently and subsequently weighted. Noteworthy, 48 h was considered to ensure a thermodynamic equilibrium of the system in terms of electrolyte saturation and chemical equilibrium of the ionic species.

The results of immersing the electrodes in the electrolyte for short periods revealed that poly(ionic liquid) binders have a higher electrolyte uptake (C-PDADMA-TFSI: 930%, C-PMTFSI-Li: 711%) than C-PVDF (290%) based electrodes. These values are associated with the low polarity and poor wettability of C-PVDF, which limit the diffusion of the electrolyte along the electrode, in comparison with poly(ionic liquid) binders. This behavior is in agreement with other works, showing a dependence between the amount of electrolyte

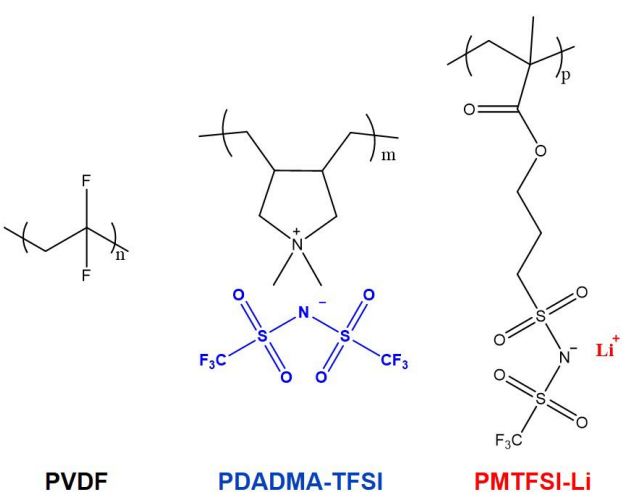


Figure 1. Chemical structure of the studied binders: a) polyvinylidene fluoride (PVDF, Solef® 5130), poly(diallyldimethylammonium bis(trifluoromethanesulfonyl)imide (PDADMA-TFSI), and poly(lithium 1-[3-(methacryloyloxy) propylsulfonyl]-1-(trifluoromethanesulfonyl)) (PMTFSI-Li).

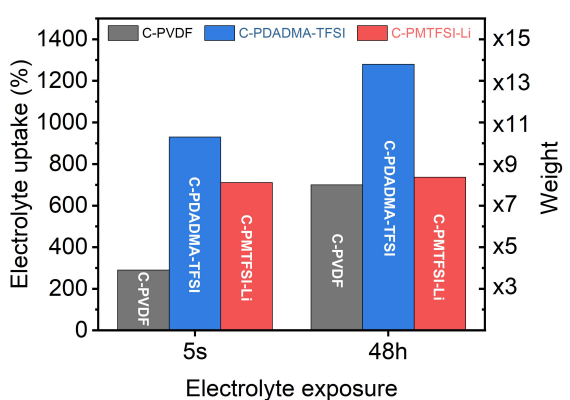


Figure 2. Electrolyte uptake of LFP/C65/binder 80/10/10 wt.% electrodes using PVDF, PDADMA-TFSI and PMTFSI-Li binders after 5 seconds and 48 h of immersion time in 1 M LiTFSI in DOL:DME (1:1 v/v) fresh electrolyte.

absorbed by the electrode and the electrolyte-binder affinity, where polar binders improve wettability and overall ionic mobility across the electrode.^[23,24]

Once the thermodynamic equilibrium was reached, the results after 48 h revealed that C-PDADMA-TFSI (1280%), C-PMTFSI-Li (736%) and C-PVDF (700%) electrodes had adsorbed respectively 74%, 97%, and 40% of their total electrolyte adsorption capacity in the first 5 seconds of wetting. Interestingly, C-PMTFSI-Li led to much faster absorption of electrolyte. Despite C-PVDF and C-PMTFSI-Li showed a similar electrolyte uptake capacity after 48 h, C-PDADMA-TFSI demonstrated a capacity to hold significantly higher amounts of liquid electrolyte (580% more compared to PVDF), which will have an impact on the battery performance as discussed in the following Sections by facilitating ion transport through the electrode.

Electrochemical characterization

To assess the effect of electrolyte uptake and free ions (either TFSI⁻ or Li⁺) on the redox reaction kinetics of the cathode, Li||LFP cells with the three different binders were studied by cyclic voltammetry. In Figure 3, peaks related to LiFePO₄/FePO₄ redox reaction are observed in the range of 2.8–3.8 V. Nonetheless, the oxidation-reduction peak positions vary among different binders and it can be seen that PMTFSI-Li binder offers the best environment for the redox reaction to occur showing the sharpest and highest peaks. As a result, the observed difference between reduction and oxidation peak potentials, called peak-to-peak separation, were 179, 189, and 209 mV for C-PMTFSI-Li, C-PVDF, and C-PDADMA-TFSI, respectively. Similar behavior was observed for other Li⁺ conducting polymer electrolytes.^[17,25] These results evidence that the redox reaction is more favored and reversible for C-PMTFSI-Li because it represents a Li⁺ source for the active material, providing readily available Li⁺ for the reduction reaction of

FePO₄ to LiFePO₄. On the contrary, C-PDADMA-TFSI shows the highest peak-to-peak separation involving slower kinetics, probably due to the ionic interactions of TFSI⁻ anions in the binder and Li⁺ cations involved in the redox reaction. Whereas PVDF binder, being a neutral polymer, is in the middle of both scenarios. Furthermore, higher oxidation current densities were obtained with C-PMTFSI-Li (0.91 A g⁻¹) in comparison with C-PVDF and C-PDADMA-TFSI (0.89 and 0.85 A g⁻¹).

Rate-capability and long-term tests

After 10 h of OCV to guarantee the equilibrium of the cells, fresh cells were cycled at different current densities and subsequently at 1 C for 500 cycles (Figure 4a). C-PMTFSI-Li electrodes provided higher capacity values than C-PDADMA-TFSI and C-PVDF, in all the studied C-rates, reaching the theoretical capacity density ($170.3 \pm 0.8 \text{ mAh g}^{-1}$) at C/10 and outstanding values at 10 C ($100.6 \pm 0.5 \text{ mAh g}^{-1}$), due to the availability of Li⁺ in PMTFSI-Li binder promoting the redox reaction of LFP, in accordance to the trend observed in the potentiostatic experiments and with other lithium single-ion conducting binders.^[17,19] In accordance with the cyclic voltammetry results, C-PVDF remained in second place providing a capacity density of $156.1 \pm 1.5 \text{ mAh g}^{-1}$ at low rate (C/10), followed by PDADMA-TFSI ($146.7 \pm 1.2 \text{ mAh g}^{-1}$ at C/10). Nonetheless, at high C-rates (10 C) C-PDADMA-TFSI reached values of $87.7 \pm 0.2 \text{ mAh g}^{-1}$ slightly surpassing C-PVDF ($87.2 \pm 0.3 \text{ mAh g}^{-1}$). This phenomenon, even if close values of capacities are implied, becomes significant when observing the voltage profiles. When the cells were cycled at C/10 (Figure 4b) low and almost indistinguishable overpotentials were observed in the three cases. At this rate, the charge/discharge process is governed by reaction kinetics offered by the different ionic environments, and it followed cyclic voltammetry study: C-PMTFSI-Li > C-PVDF > C-PDADMA-TFSI. However, when the C-rate was increased, large overpotentials were observed due to mass transfer limitations (Figure 4c), specially for C-PVDF. C-PMTFSI-Li exhibited the smallest polarization, due to its structural characteristics that promote Li⁺ transport, as described for other polymeric systems with single lithium-ion conducting properties.^[17,18,25] C-PDADMA-TFSI could also slightly mitigate this effect by facilitating the Li⁺ mobility since more electrolyte uptake was observed for this electrode, but also by interaction with free TFSI⁻ ions of the binder. Similar works have already demonstrated the benefits of free anions in terms of polarization.^[21,26] Finally, C-PVDF showed the highest polarization at high current densities.

In the long-term cycling, after 535 cycles, C-PMTFSI-Li and C-PDADMA-TFSI showed stable cycling and high capacity retention (140.5 mAh g^{-1} , 96%, and 130.5 mAh g^{-1} , 99%, respectively), while C-PVDF delivered 138.5 mAh g^{-1} , 99% in cycle number 494 before fading. Subsequently, cells were opened to evaluate electrode deterioration after rinsing the cycled electrodes with DOL/DME (1/1) to remove the adsorbed salt excess. Figure 5 shows the cross-sectional SEM images of the cathodes before and after cycling, where C-PVDF based

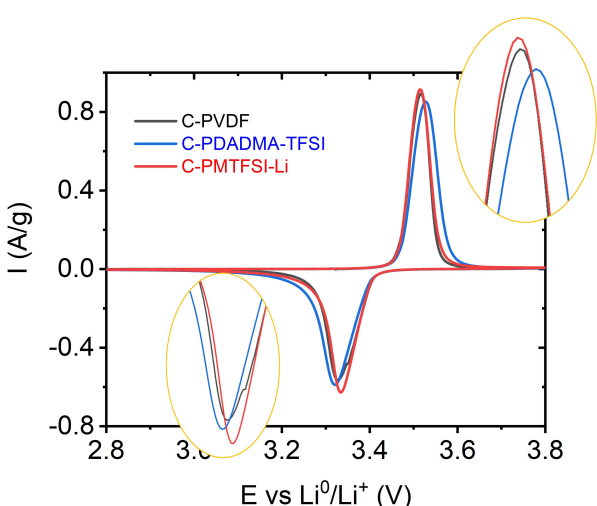


Figure 3. Cyclic voltammograms of Li||LFP cells with different cathode binders at 0.1 mVs^{-1} .

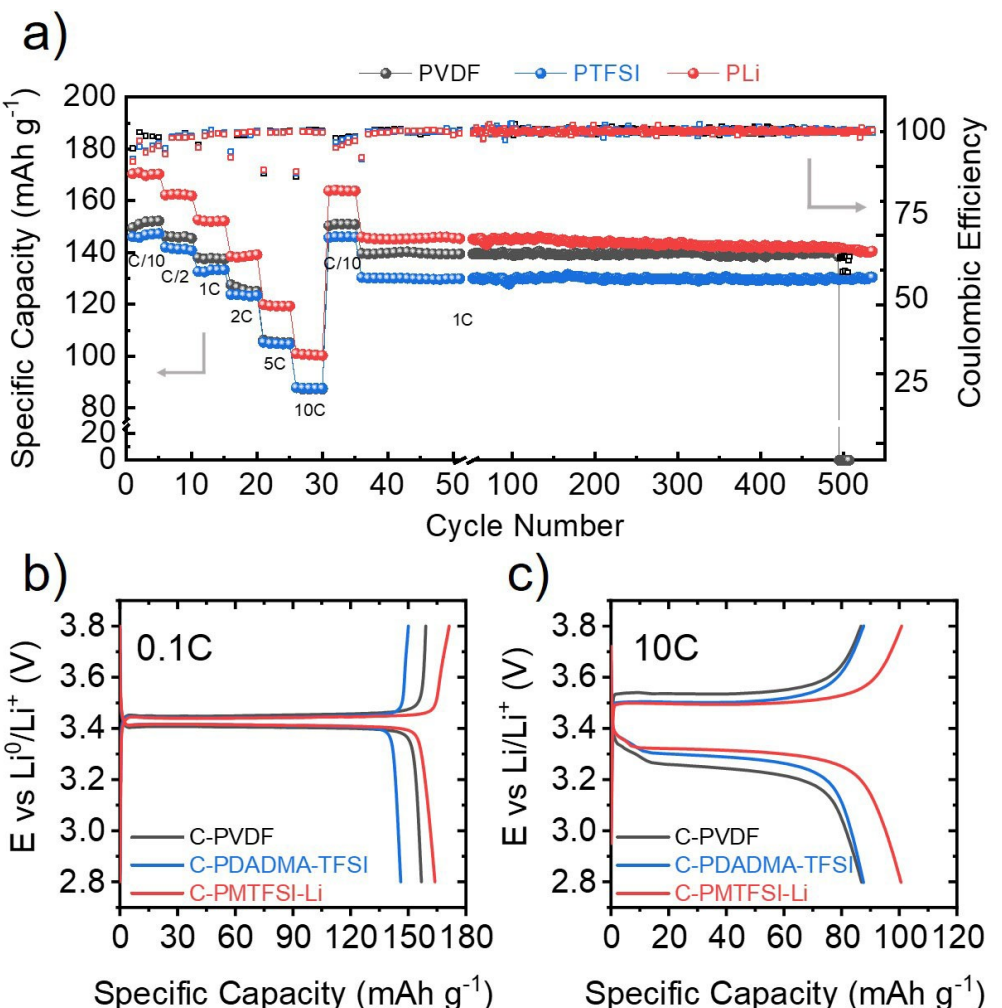


Figure 4. a) Rate capability and long-term cycling of Li||LFP cells using different binders: C–PVDF, C–PDADMA–TFSI, C–PMTFSI–Li as shown in Figure legend. Voltage profiles of the cells at b) 0.1 C and c) 10 C rates at room temperature.

cathode showed a more damaged structure than the ones based on C–PDADMA–TFSI and C–PMTFSI–Li.

In order to gain insight into the potential application of these polymer binders, electrodes with higher loadings ($4 \text{ mg}_{\text{LFP}} \text{ cm}^{-2}$) were prepared and analyzed. After cycling under the same conditions of rate capability (Figure S8), C–PMTFSI–Li and C–PDADMA–TFSI electrodes were able to cycle stably at high current density of 10 C, while C–PVDF started to fail at that current density. Similar trend was observed for the low loading electrodes in the long cycling test at 1 C current density (Figure 4a), highlighting the superior performance of C–PMTFSI–Li based electrode. Further characterization was carried out using the lower-loading electrodes to avoid the influence of resistances and diffusion limitations present in the 4 mg cm^{-2} electrodes.

Electrochemical impedance spectroscopy (EIS)

In order to get a deeper understanding of the systems, EIS was performed to elucidate different resistances and capacitive

contributions involved in the electrode composite. However, as explained by Suarez-Hernandez et al., the EIS spectrum of a battery is influenced by several factors (potential, additives, state of charge (SOC), etc.).^[18] For this reason, a protocol was designed to collect EIS spectra at the same voltage and SOC = 50% to see the effect of the different binders under the same conditions (see Figure S9). Firstly, fresh cells were assembled and exposed to 18 h of OCV, observing different voltage evolutions. Secondly, the cells were galvanostatically cycled by applying a low current density, corresponding to a C-rate of C/10 and 5 min of OCV before EIS measurement to ensure steady-state conditions at SOC = 50% when charging and discharging in the third cycle.

The effect of the voltage on EIS spectrum has been studied addressing the changes in the concentration of the ionic species.^[27] In this work, even if all the cells started at the same potential (3.4 V), different OCV profiles were obtained for each binder and hence, a comparison between cells in a specific time would be influenced by its potential (see Figure S10). In this step, EIS spectra were taken every two hours to observe the evolution of the Nyquist plot to larger semicircles and more

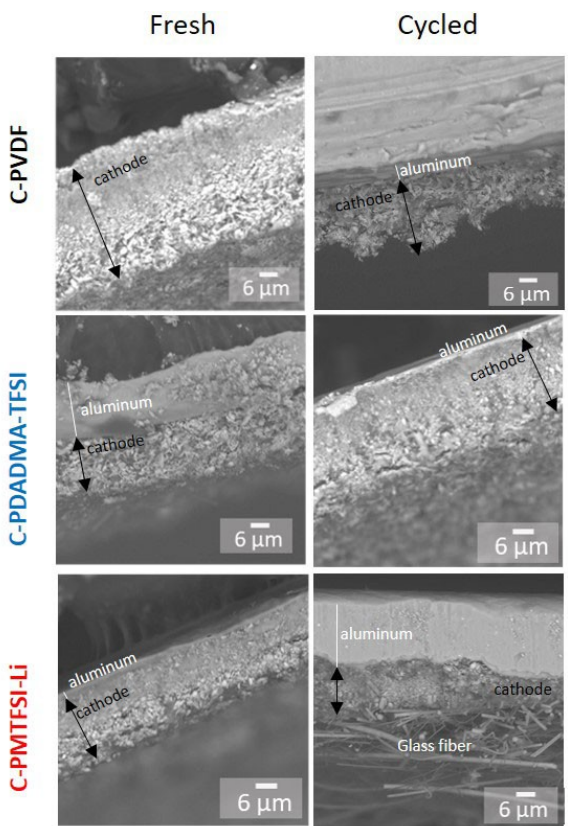


Figure 5. Cross-sectional SEM images of fresh electrodes and after 500 cycles of LFP-based cathodes using different binders as labelled. Black arrows and white lines represent the cathode and aluminum edges, respectively.

capacitive shape at low frequencies given by the accumulation of charged species inside the electrode as can be observed from Figure S11. From these results it can be concluded a faster stabilization occurred in the cells based on ionic binder, obtaining capacitive EIS spectra at low frequencies and reaching the voltage plateau at shorter times, specially for C–PMTFSI–Li being almost instantaneous, in good agreement with the wettability test.

The next step, (EIS at SOC=50% of charge and discharge) is depicted in Figure 6. The used equivalent circuit (ecc) (Figure 6a) was proposed by similar previous works to fit the data (Table S1) because of its confirmed accuracy in LFP-based cells and quality of extracted information. In these Nyquist plots, firstly the solution electrolyte resistance is labelled as R_s . Subsequently, at high frequencies, can be found a depressed semicircle that corresponds mostly to the interfacial charge transfer resistance (R_{ct}), in parallel with the double-layer capacitance (C_{dl}), together with a small contribution of the contact between particles resistance (R_c) and respective capacitance (C_c). At intermediate frequencies we observe the resistance related to the lithiation process of the active material (R_{lr}) and its associated lithiation capacitance (C_{Li+}), which is related to the amount of Li^+ out of the active material particle (in this case LFP). Finally, at very low frequencies a capacitive shape appears as a consequence of Li^+ intercalation in the phosphate matrix quantified by its chemical capacitance (C_μ).

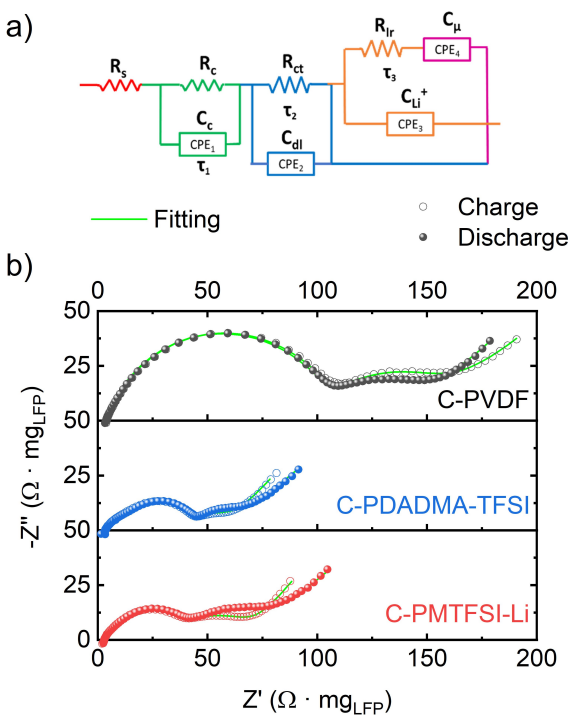


Figure 6. a) Proposed equivalent circuit and b) EIS spectra of $\text{Li} \parallel \text{LFP}$ cells with different binders at $\text{SOC}=50\%$; obtained for charge and discharge processes are identified by empty circles and filled spheres respectively, and green lines correspond to obtained fitting.

This parameter counts the ease for Li^+ to reach the active material.

The cells containing the three different binders presented significantly different Nyquist plots, while the impedance spectra at charged and discharged states were also different (Figure 6b). Even if an identical shape was observed during charge and discharge until medium frequencies in the three cells, more capacitive spectra were exhibited at low frequencies when cells were discharging since they were accumulating Li^+ . Table S1 summarizes the extracted data from the equivalent circuit for these parameters. Despite using the same electrolyte for the three cells, R_s was found to vary among the different systems: 4.2 (C–PVDF), 3.8 (C–PDADMA–TFSI) and 2.8 (C–PMTFSI–Li) $\Omega \cdot \text{mg}_{\text{LFP}}$; suggesting a certain interaction between the electrolyte and the ionic binder that improves the ion mobility.

Then, if we consider the behavior upon discharging at high frequencies, a higher R_c ($8.1 \Omega \cdot \text{mg}_{\text{LFP}}$) was observed when C–PDADMA–TFSI was used according to the higher porosity observed by SEM while the use of PMTFSI–Li binder led to lower R_c ($3.5 \Omega \cdot \text{mg}_{\text{LFP}}$). Subsequently, R_{ct} was remarkably lower in the case of C–PDADMA–TFSI ($34.2 \Omega \cdot \text{mg}_{\text{LFP}}$) and C–PMTFSI–Li ($36.2 \Omega \cdot \text{mg}_{\text{LFP}}$) compared with C–PVDF ($102.5 \Omega \cdot \text{mg}_{\text{LFP}}$) which enabled a faster ion delivery from the electrolyte corroborating lower charge transfer limitations when PDADMA–TFSI and PMTFSI–Li binders were used. Apart from, C–PMTFSI–Li and C–PDADMA–TFSI showing very low charge transfer resistances, they also exhibit the highest C_{dl} (4.8×10^{-3} and $3.7 \times 10^{-3} \text{ F g}_{\text{LFP}}^{-1}$), meaning a higher amount of

charged species in the double layer as expected, whereas C–PVDF has a lower C_{dl} $1.6 \times 10^{-3} \text{ F g}_{\text{LFP}}^{-1}$.

At low frequencies, C–PDADMA–TFSI based cell showed the lowest R_{lr} ($18.1 \Omega \cdot \text{mg}_{\text{LFP}}$) indicating the fastest medium for the Li^+ ion to reach the active center, followed by C–PMTFSI–Li and finally C–PVDF. However, the values of C_μ parameter is aligned with the CV experiments, showing a more hindered reaction for C–PDADMA–TFSI ($15.4 \text{ F g}_{\text{LFP}}^{-1}$) in comparison with C–PVDF and C–PMTFSI–Li, (27.7 and $27.3 \text{ F g}_{\text{LFP}}^{-1}$, respectively). Even if C–PVDF and C–PMTFSI–Li presented very similar C_μ when they were discharging, C–PMTFSI–Li exhibited a higher value when it was charging ($41.1 \text{ F g}_{\text{LFP}}^{-1}$) in comparison with C–PVDF ($32.2 \text{ F g}_{\text{LFP}}^{-1}$) meaning a more effective galvanostatic charge storage (Figure 7iii). These values are in agreement with C_{Li^+} in each case, where in C–PDADMA–TFSI the cell accumulates more Li^+ ions that did not reach the active material ($0.71 \text{ F g}_{\text{LFP}}^{-1}$), while C–PVDF and C–PMTFSI–Li presented lower capacitance values (0.45 and $0.47 \text{ F g}_{\text{LFP}}^{-1}$, respectively). These values at low frequencies can be understood if we consider the interactions that may occur between Li^+ ions and free TFSI⁻ counterions of C–PDADMA–TFSI, which may increase Li^+ mobility and retain its entrance to active centers as proposed by the scheme (Figure 7i and ii). Nonetheless, once again C–PMTFSI–Li exhibited a more effective galvanostatic charge with a lower amount of accumulated Li^+ ($0.40 \text{ F g}_{\text{LFP}}^{-1}$) in comparison with C–PVDF ($0.46 \text{ F g}_{\text{LFP}}^{-1}$) since the release of Li^+ from the active material might be boosted by repulsion with mobile Li^+ associated with the PMTFSI–Li binder (see Figure 7iii and iv). Overall, EIS results suggested a favored medium for mass transport when PDADMA–TFSI binder was used but at the same time, the Li^+ -TFSI⁻ interactions hinder the redox reaction. Moreover, the use PMTFSI–Li binder provided the ideal scenario with low charge transference resistance and efficient galvanostatic charge and discharge.

After EIS measurements, the same cells were cycled at 2 C for 40 cycles to promote cell polarization and subsequently

opened inside an argon-filled glovebox. SEM images of cross-sectional lithium were taken to observe anode deterioration. As is shown in Figure 8, a huge amount of mossy lithium layer was formed onto the anode in C–PVDF cell which could shorten its cycle life while C–PDADMA–TFSI cell, because of its enhanced mass transport during cycling, mitigated that growth. Interestingly, no mossy lithium was observed in the C–PMTFSI–Li cell, which apparently, limited the deterioration of the anode preventing cell failure in the presence of ionic binders as shown in Figure 4. Therefore, similarly to what occurs in the field of electrolytes, the single lithium-ion polymer PMTFSI–Li, when used as binder, may prevent concentration gradients through restricting anion motion into the cathode and thereby regulating ion concentration in the cell; this interestingly seems to correlate with more homogeneous lithium plating. In a PVDF scenario, cell charging (i.e., Li metal deposition) will lead to typical concentration gradients (as the anions move into the electrode) and subsequent heterogeneous plating onto the lithium metal anode as represented in Figure 7(v). In contrast, PDADMA–TFSI and PMTFSI–Li based electrodes limited this problem by acting as ion buffers by restraining the polarization of the TFSI⁻ counterion. PDADMA–TFSI system already contains a high population of TFSI⁻ anions impeding its diffusion (Figure 7vi), whereas PMTFSI–Li may repulse TFSI⁻ anions electrostatically by interaction with negatively charged polymer chain (Figure 7vii).

Optimization

The PMTFSI–Li used so far was synthesized following the procedure of Olmedo-Martínez et al., targeting a molecular weight (M_w) of 50 kDa.^[28] However, when the polymer was casted for higher loading devices ($> 4 \text{ mg}_{\text{LFP}} \text{ cm}^{-2}$), the electrode integrity was lost compromising the battery performance. Therefore, two new PMTFSI–Li polymers were synthesized

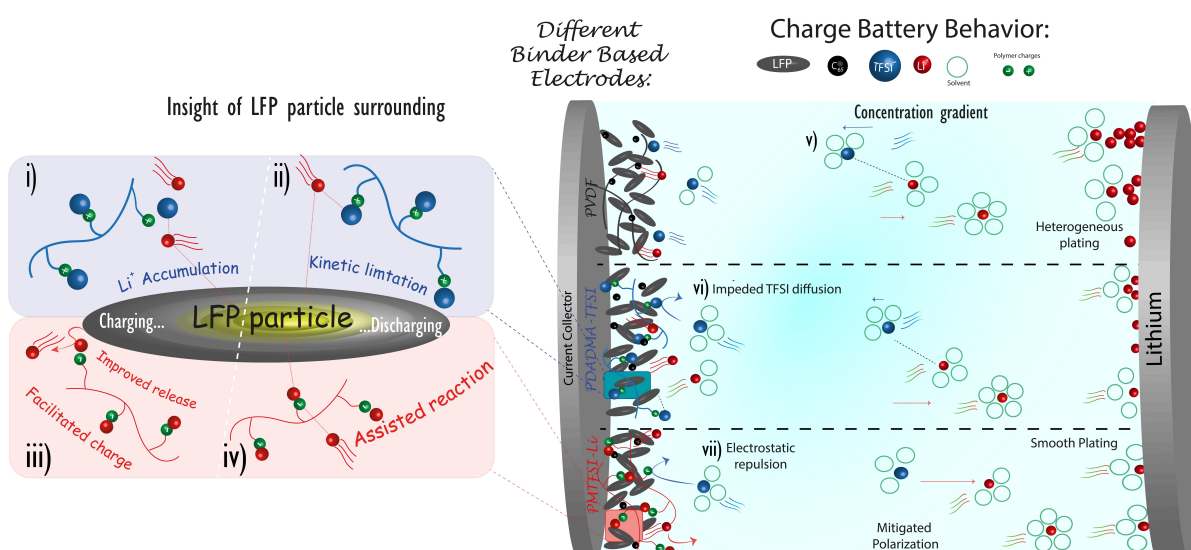


Figure 7. Proposed scheme of the ionic interactions between charged species for C–PVDF, C–PDADMA–TFSI, and C–PMTFSI–Li cells.

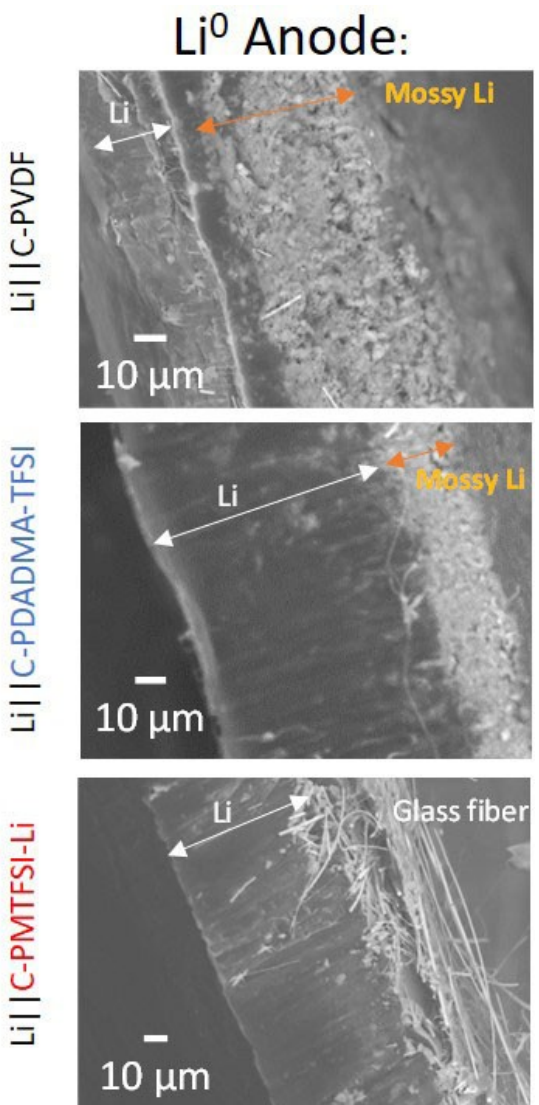


Figure 8. Cross-sectional SEM images of lithium metal anode from different $\text{Li}||\text{LFP}$ cells (as labeled in the figure) after being cycled at 2 C for 40 cycles.

targeting higher M_w (250 and $>2,000$ kDa), and subsequently employed in LFP formulations with similar conditions in order to investigate the effect of the molecular weight binder on the binding properties and battery performance. Afterwards, the effect of the electrolyte employed was analyzed for high loading electrodes, since an ideal electrolyte should not only provide high ionic conductivity, but also be stable at high current densities, which are required for fast charge-discharge cyclings and high-loading devices. These properties are key for the lifespan, energy and power density of the devices.

Effect of M_w

From the point of view of electrode casting, mass loadings of $11 \text{ mg}_{\text{LFP}} \text{ cm}^{-2}$ were achieved using 250 kDa PMTFSI–Li poly(ionic liquid) with no significant cracks as observed in

Figure S12. When employing 50 and 2,000 kDa polymers, the electrodes started cracking at 6.6 and $4.3 \text{ mg}_{\text{LFP}} \text{ cm}^{-2}$. These results indicate that, either PMTFSI–Li ($>2,000$ kDa) forms too rigid coatings or the presence of residual emulsifiers from the polymerization is affecting the properties of the polymer. The enhanced mechanical properties by increasing the M_w of PMTFSI–Li were confirmed by dynamic mechanical analysis (DMA) obtaining storage modulus values at 40°C of 2.1×10^7 , 3.4×10^7 and $4.7 \times 10^7 \text{ Pa}$ for 50, 250 and $>2,000$ kDa respectively (see Figure S13).

Subsequently, the cathodes based on PMTFSI–Li poly(ionic liquid) of different molecular weights (termed C-50, C-250 and C-2,000) were subsequently cycled using 1 M LiTFSI (DOL/DME 1:1 v/v) against lithium metal in a rate capability test (Figure S14a). From Figure S14(b), it can be seen that the specific capacity delivered by the different PMTFSI–Li-based cells at 1 C and different mass loadings. The three cathodes (C-50, C-250 and C-2,000) delivered roughly the same specific capacity at 1 C when using low loadings (138 mAh g^{-1} with $3\text{--}3.7 \text{ mg}_{\text{LFP}} \text{ cm}^{-2}$), but the capacity rapidly decreased when using higher mass loading electrodes (117.4 mAh g^{-1} with $10.8 \text{ mg}_{\text{LFP}} \text{ cm}^{-2}$). In agreement with the quality of the slurries observed before, C-250 provided higher specific capacities in all the range measured. Figure 9a depicts the specific capacity of $\sim 4.5 \text{ mg}_{\text{LFP}} \text{ cm}^{-2}$ cells at different C-rates, reflecting a similar performance for different molecular weights of PMTFSI–Li at low C-rate (161 mAh g^{-1} at C/10). However, when the electrodes were pushed to cycle at higher C-rates, C-250 remained as the best electrode delivering values of 78.6 mAh g^{-1} at 10 C. Therefore, the quality of the electrode seems not only to affect the capacity obtained at high mass loadings, when the fissures are evident; but also the rate capability.

Effect of electrolyte

In order to obtain a stable cycling for high loading electrodes, different electrolytes were tested in $\text{Li}||\text{LFP}$ cells: 1 M LiTFSI in DOL/DME (1:1 v/v), 1 M LiTFSI in EC/DEC (1:1 v/v) and 1 M LiPF₆ in EC/DEC (1:1 v/v) at 1 C (Figure S15). The results show slightly higher capacities delivered when using 1 M LiTFSI DOL/DME (1:1 v/v), but rapid fade after 20 cycles. In contrast, the electrolytes containing EC/DEC solvent present much more stable cycling (100 cycles) delivering $\sim 113 \text{ mAh g}^{-1}$ at 1 C (1.2 mAh cm^{-2}), revealing a big impact of the solvent on the cell performance and not so much the nature of these salts (LiTFSI and LiPF₆).

1 M LiPF₆ EC/DEC (1:1 v/v) was selected as electrolyte to compare against conventional PVDF for the exhibited stability and wide use in LIBs.^[29] Figure 9b shows the cycling of $\text{Li}||\text{LFP}$ cells containing PVDF and PMTFSI–Li of 250 KDa as binders for the cathodes (C-250) at 1 C. PVDF-based cell faded after 100 cycles delivering $119.5 \pm 1.9 \text{ mAh g}^{-1}$ (0.95 mAh cm^{-2}) while C-250 exhibited very stable cycling of $130.4 \pm 1.4 \text{ mAh g}^{-1}$ (0.98 mAh cm^{-2}), in good agreement with the first part of this study.

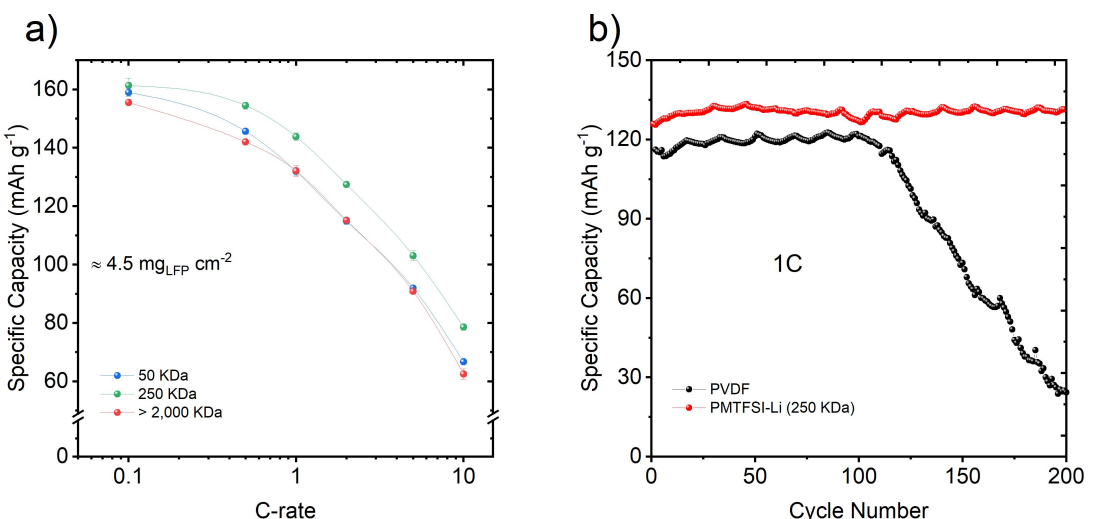


Figure 9. a) Specific capacity of Li | 1 M LiTFSI (DOL/DME) | LFP cells using PMTFSI–Li of different M_w as binders with $4.5 \text{ mg}_{\text{LFP}} \text{ cm}^{-2}$ as function of C-rate. b) Cycling of Li | 1 M LiPF₆ EC/DEC (1/1 v:v) | LFP cells at 1 C using PVDF and PMTFSI–Li (250 kDa) as binders. Mass loading electrodes $\sim 7.5 \text{ mg}_{\text{LFP}} \text{ cm}^{-2}$ (practical $\sim 1 \text{ mAh cm}^{-2}$).

Conclusion

In this work, we studied the impact of using different types of poly(ionic liquid) polymers as binders in LFP cathodes for LMB and compared their performances with conventional PVDF binder. The cell with the innovative C-PMTFSI–Li cathodes exhibited optimum conditions for the LiFePO₄ redox reaction and consequently the best discharge capacity ($170.3 \pm 0.8 \text{ mAh g}^{-1}$) at C/10. An outstanding capacity at 10 C ($100.6 \pm 0.5 \text{ mAh g}^{-1}$) and stable cyclability with a capacity retention of 96% (140.5 mAh g^{-1}) after > 500 cycles at 1 C were obtained. When comparing C-PDADMA-TFSI and C-PVDF, at low C-rate C-PVDF had higher capacities than C-PDADMA-TFSI, but as the C-rate was increased, mass transport limitations limited the performance of C-PVDF, particularly with high loading electrodes, producing large overpotentials. Transport limitations were identified by EIS through significant charge transfer resistances. Moreover, C-PVDF cell showed a more deteriorated cathode after long-term cycling in contrast to the stable cycling of C-PDADMA-TFSI and C-PMTFSI–Li as a consequence of an efficient charge transfer through Li⁺ interaction with mobile free TFSI anions. Furthermore, when fresh cells were cycled at 2 C for 40 cycles after EIS measurements to promote cell polarization, no mossy lithium was observed in the anode in the C-PMTFSI–Li cell, while a small layer was found in C-PDADMA-TFSI cell and a large amount of mossy lithium was observed for C-PVDF cells, being probably the cause of fading. Interestingly, the poly(ionic liquid) binders showed a more homogeneous plating, particularly the single-ion conducting polymer PMTFSI–Li. This intriguing observation was explained by the interaction binder-electrolyte despite further work should be done to fully understand this phenomenon. Therefore, the use of poly(ionic liquid) binders is proposed for enhanced and longer-life batteries and greener processing since PDADMA-TFSI and PMTFSI–Li are

also soluble in acetone and water respectively, potentially avoiding the use of toxic NMP for processing and recycling for a second life application. Finally, PMTFSI–Li was synthesized with higher M_w to reach mass loadings in the range of $11 \text{ mg}_{\text{LFP}} \text{ cm}^{-2}$; while still obtaining high specific capacities ($130.4 \pm 1.4 \text{ mAh g}^{-1}$ with PMTFSI–Li M_w of 250 kDa), in comparison with conventional PVDF ($119 \pm 1.9 \text{ mAh g}^{-1}$) enabling the practical application of this poly(ionic liquid) as binder in cathode formulations.

Experimental Section

Materials. PVDF Solef® 5130 (1,000-1,100 kg mol⁻¹) was used as a reference binder. The synthesis of PDADMA-TFSI was proceeded by ion exchange using poly(dyallydimethylammonium chloride) (400–500 kg mol⁻¹) and KTFSI as reported in literature (see ¹H NMR and ¹⁹F NMR (400 MHz, acetone-d₆) in Figures S1 and S2; and FTIR in Figure S5 where the signals correspond as labelled in the spectra).^[30] N-methyl-2-pyrrolidinone (NMP, 99%, Sigma-Aldrich), anhydrous 1,3-dioxolane (99.8%, Sigma-Aldrich), anhydrous dimethoxy ethane (99.5%, Sigma-Aldrich), lithium bis(trifluoromethanesulfonyl)imide (LiTFSI, 99%, Iolitec), conductive carbon (Super C65, Timcal), lithium iron phosphate (LiFePO₄, Alerees) were used without further treatment.

Synthesis of PMTFSI–Li. PMTFSI–Li was synthesized by using reversible addition-fragmentation chain transfer (RAFT) polymerization of commercial lithium 1-[3-methacryloyloxy] propylsulfonyl]-1-(trifluoromethanesulfonyl) imide monomer (LiMTFSI) (Specific Polymers) targeting 50 kDa (see ¹H NMR and ¹⁹F NMR (400 MHz, acetone-d₆) in Figures S3 and S4; and FTIR in Figure S5 where the signals correspond as labelled in the spectra); and by inverse emulsion polymerization (IEP) for $> 2,000$ kDa according to already reported procedures.^[28] For the synthesis of PMTFSI–Li of 250 kDa, free radical polymerization (FRP) was employed. A degassed solution of LiMTFSI (1.5 g 4.31 mmol) and AIBN (1 mg, 0.061 mmol) in 5 g DMF was polymerized in a Schlenk tube vigorously stirring at 90 °C under argon atmosphere for 8 h. The obtained polymer was purified by precipitation in cold diethyl ether and subsequently dried at 60 °C under high vacuum overnight. Table 1 summarizes

Table 1. SEC of the synthesized polymers at 25 °C, 0.1 M LiCl in water.				
Label	M_n [kg mol ⁻¹]	M_w [kg mol ⁻¹]	\overline{D}	Ref.
50	44.9	59.2	1.32	[28]
250	88.3	259	2.934	This work
>2,000	-	-	-	[28]

the data obtained by size exclusion chromatography (SEC) in comparison with the reported procedure. The highest M_w polymer was out of the range of the SEC columns available and a M_w of >2,000 is stimated.

Electrode preparation. The slurries were prepared by dissolving the binder first in NMP in a small beaker and subsequently addition of C65 and LFP. After one day stirring, the viscous slurry was coated onto carbon-coated aluminum foil (current collector) with the aid of an automatic doctor blade (NEURTEK Instruments) and it was left drying at room temperature for 12 h. Finally, disks of 11 mm diameter were punched and further dried at 60 °C under vacuum for 24 h prior characterization. To evaluate the intrinsic properties of binders, thin electrodes were prepared (between 1.0 and 2.3 mg_{LFP} cm⁻²). For the high loading electrodes, slurries were mixed with the aid of a speed mixer (FlackTek) and subsequently coated at different thicknesses 75–250 µm.

Electrolyte uptake. Pristine electrodes (LFP/C65/binder 80/10/10 wt %, 11 mm diameter), prepared as indicated in the supplementary information, were soaked separately in fresh electrolyte (0.5 mL) for short (5 seconds) and long (48 h) immersion times in closed vials independently and subsequently weighted. Noteworthy, 48 h was considered to ensure a thermodynamic equilibrium of the system in terms of electrolyte saturation and chemical equilibrium of the ionic species.

Cell assembly. LFP cathode (11 mm diameter) with loading between 1.0–2.3 mg_{LFP} cm⁻² of active material were prepared as detailed in supplementary information. Li||LFP cells were assembled in CR2032 coin cells inside Ar glovebox, by firstly cleaning Li ribbons with cyclohexane and a nylon brush prior punching 12 mm disks and using 120 µL of 1 M LiTFSI/DOL-DME (1:1) as electrolyte in glass microfiber separators.

Electrochemical measurements. Rate capability for assembled cell was performed constant current at (0.1 C, 0.5 C, 1 C, 2 C, 5 C and 10 C) on a Neware battery cycles, whereas VMP-3 potentiostat (Biologic) was used to carry out further electrochemical characterization. Cyclic voltammetry (CV) was used in the range of 2.8–3.8 V at 0.1 mVs⁻¹. Electrochemical impedance spectroscopy (EIS) was employed to determine processes resistances and capacitances involved in Li||LFP cells with a perturbation of 10 mV and a frequency range from 1 MHz–0.1 Hz with a VMP-3 potentiostat (Biologic). Afterward, data were fitted in frequency, Z and –Z'' by using Zview software obtaining Chi-Squared values below 1×10^{-4} .

Dynamic mechanical analysis. Compressive mode dynamic mechanical analysis (DMA, PerkinElmer DMA8000) was used to analyze the mechanical properties of the polymers. The polymer was pressed in KBr die and dried at 70 °C under vacuum overnight to finally obtain pellets of around 1–4 mm in thickness and 0.5 cm⁻². The temperature range of DMA was 40–80 °C and the frequency was set at 1 Hz. The measurements were performed in open air.

Acknowledgements

N.C. would like to thank the University of the Basque Country (No. 823989) for funding through a specialization of research staff fellowship (ESPDOC 19/99). G. G.-G. is grateful to "Secretaría de Educación, Ciencia, Tecnología e Innovación" from Ciudad de México for a postdoctoral fellowship through grant (SECTEI/133/2019). Financial support of MCIN/AEI through project PID2020-119026GB-I00 is also acknowledged.

Conflict of Interest

The authors declare no conflict of interest.

Data Availability Statement

The data that support the findings of this study are available from the corresponding author upon reasonable request.

Keywords: cell polarization • functionalized binder • lithium-metal batteries • poly(ionic liquid) • polymer binder • selective ion-transport

- [1] H. Chen, M. Ling, L. Hencz, H. Y. Ling, G. Li, Z. Lin, G. Liu, S. Zhang, *Chem. Rev.* **2018**, *118*, 8936–8982.
- [2] C. Liu, Z. G. Neale, G. Cao, *Mater. Today* **2016**, *19*, 109–123.
- [3] H. D. Abruña, Y. Kiya, J. C. Henderson, *Phys. Today* **2008**, *61*, 43–47.
- [4] T. Placke, R. Kloepsch, S. Dühnen, M. Winter, *J. Solid State Electrochem.* **2017**, *21*, 1939–1964.
- [5] X. B. Cheng, R. Zhang, C. Z. Zhao, Q. Zhang, *Chem. Rev.* **2017**, *117*, 10403–10473.
- [6] D. Mecerreyres, L. Porcarelli, N. Casado, *Macromol. Chem. Phys.* **2020**, *221*, 1–7.
- [7] X. Qi, B. Blizanac, A. Dupasquier, M. Oljaca, J. Li, M. Winter, *Carbon* **2013**, *64*, 334–340.
- [8] K. A. Seid, J. C. Badot, O. Dubrunfaut, S. Levasseur, D. Guyomard, B. Lestriez, *J. Mater. Chem.* **2012**, *22*, 24057–24066.
- [9] D. Xu, X. Chu, Y. B. He, Z. Ding, B. Li, W. Han, H. Du, F. Kang, *Electrochim. Acta* **2015**, *152*, 398–407.
- [10] A. Eftekhari, *J. Power Sources* **2017**, *343*, 395–411.
- [11] J. Zhao, X. Yang, Y. Yao, Y. Gao, Y. Sui, B. Zou, H. Ehrenberg, G. Chen, F. Du, *Adv. Sci.* **2018**, *5*, 1700768.
- [12] D. Bresser, D. Buchholz, A. Moretti, A. Varzi, S. Passerini, *Energy Environ. Sci.* **2018**, *11*, 3096–3127.
- [13] J. Xu, S. L. Chou, Q. F. Gu, H. K. Liu, S. X. Dou, *J. Power Sources* **2013**, *225*, 172–178.
- [14] V. A. Nguyen, C. Kuss, *J. Electrochem. Soc.* **2020**, *167*, 065501.
- [15] P. R. Das, L. Komsisyska, O. Osters, G. Wittstock, *J. Electrochem. Soc.* **2015**, *162*, A674–A678.
- [16] G. Guzmán-González, G. Ramos-Sánchez, L. E. Camacho-Forero, I. González, *J. Phys. Chem. C* **2019**, *123*, 17686–17694.
- [17] L. Qiu, Z. Shao, D. Wang, F. Wang, W. Wang, J. Wang, *Carbohydr. Polym.* **2014**, *112*, 532–538.
- [18] R. Suárez-Hernández, G. Ramos-Sánchez, I. O. Santos-Mendoza, G. Guzmán-González, I. González, *J. Electrochem. Soc.* **2020**, *167*, 100529.
- [19] A. Santiago, E. Sanchez-Diez, U. Oteo, I. Aldalur, M. Echeverria, M. Armand, M. Martínez-Ibañez, H. Zhang, *Small* **2022**, *18*, 2202027.
- [20] S. B. Hong, Y. J. Lee, U. H. Kim, C. Bak, Y. M. Lee, W. Cho, H. J. Hah, Y. K. Sun, D. W. Kim, *ACS Energy Lett.* **2022**, *7*, 1092–1100.
- [21] J. S. Lee, K. Sakaushi, M. Antonietti, J. Yuan, *RSC Adv.* **2015**, *5*, 85517–85522.
- [22] S. Dühnen, J. Betz, M. Kolek, R. Schmuck, M. Winter, T. Placke, *Small Methods* **2020**, *4*, 2000039.

- [23] N. S. Choi, Y. G. Lee, J. K. Park, *J. Power Sources* **2002**, *112*, 61–66.
- [24] B. Lestriez, *Comptes Rendus Chim.* **2010**, *13*, 1341–1350.
- [25] L. Xie, L. Zhao, J. Wan, Z. Shao, F. Wang, S. Lv, *J. Electrochem. Soc.* **2012**, *159*, A499–A505.
- [26] Y. Y. Lin, Y. M. Chen, S. S. Hou, J. S. Jan, Y. L. Lee, H. Teng, *J. Mater. Chem. A* **2017**, *5*, 17476–17481.
- [27] N. Vicente, M. Haro, D. Cíntora-Juárez, C. Pérez-Vicente, J. L. Tirado, S. Ahmad, G. García-Belmonte, *Electrochim. Acta* **2015**, *163*, 323–329.
- [28] J. L. Olmedo-Martínez, L. Porcarelli, L. Porcarelli, Á. Alegría, Á. Alegría, D. Mecerreyres, A. J. Müller, *Macromolecules* **2020**, *53*, 4442–4453.
- [29] Q. Li, J. Chen, L. Fan, X. Kong, Y. Lu, *Green Energy & Environ.* **2016**, *1*, 18–42.
- [30] R. Del Olmo, N. Casado, J. L. Olmedo-Martínez, X. Wang, M. Forsyth, *Polymers (Basel.)* **2020**, *12*, 1981.

Manuscript received: December 1, 2022
Revised manuscript received: December 27, 2022
Accepted manuscript online: December 30, 2022
Version of record online: January 18, 2023